THE AMERICAN SOCIETY OF MECHANICAL ENGINEERS
345 E. 47th St., New York, N.Y. 10017

98-GT-190

TURBULENCE SPECTRA AND LENGTH SCALES MEASURED IN FILM COOLANT FLOWS EMERGING FROM DISCRETE HOLES

Steven W. Burd and Terrence W. Simon

Heat Transfer Laboratory
University of Minnesota
Minneapolis, MN 55455 U.S.A.

ABSTRACT

To date, very little attention has been devoted to the scales and turbulence energy spectra of coolant exiting from film cooling holes. Length scale documentation and spectral measurements have primarily been concerned with the freestream flow with which the coolant interacts. Documentation of scales and energy decomposition of the coolant flow leads to more complete understanding of this important flow and the mechanisms by which it disperses and mixes with the freestream. CFD modeling of the emerging flow can use these data as verification that flow computations are accurate. To address this need, spectral measurements were taken with single-sensor, hot-wire anemometry at the exit plane of film cooling holes. Energy spectral distributions and length scales calculated from these distributions are presented for film cooling holes of different lengths and for coolant supply plenums of different geometries. Measurements are presented on the hole streamwise centerline at the center of the hole, one-half diameter upstream of center, and one-half diameter downstream of center. The data highlight some fundamental differences in energy content, dominant frequencies, and scales with changes in the hole and plenum geometries. Coolant flowing through long holes exhibits smoothly-distributed spectra as might be anticipated in fully-developed tube flows. Spectra from short-hole flows, however, show dominant frequencies.

NOMENCLATURE

D	Film cooling hole, pipe, or cylinder diameter (m)
$E(\kappa)$	Wave number based power spectral density (m^3/s^2)
$E(f)$	Frequency based power spectral density (m^2/s)
f	Frequency (Hz)
k	Turbulence kinetic energy (m^2/s^2)
L	Film cooling hole length (m)
L_u	Energy or dissipation turbulent length scale (m)
I	Coolant-to-mainstream momentum flux ratio
P	Frequency-weighted spectra, $E(f)\times f/(u_{eff})^2$
Re	Reynolds number based on U_∞ and D
Re_D	Reynolds number based on U_{hole} and D
St	Strouhal number (fD/U_{eff})
St_D	Strouhal number (fD/U_{hole})
t	Wall thickness of hole extension tube (m)
U_{eff}	Mean effective velocity (m/s)
U_{hole}	Bulk mean film cooling hole (pipe) velocity (m/s)
U_∞	Freestream velocity (m/s)
VR	Coolant-to-mainstream velocity ratio
u_{eff}	rms fluctuation about U_{eff} (m/s)
x	Streamwise distance from hole center (m)
y	Wall-normal distance (m)
z	Lateral distance from hole center (m)

Greek

δ^*	Boundary layer displacement thickness (m)
δ_{99}	Boundary layer thickness (99%) (m)
$\Delta \dot{m}$	Mass flow uncertainty (95% confidence) (kg/s)
ε	Dissipation rate (m^2/s^3)
η	Kolmogorov or microscale of turbulence (m)
κ	Wave number (m^{-1})
Λ	Integral length scale (m)
ν	Kinematic viscosity (m^2/s)
θ	Boundary layer momentum thickness (m)

Presented at the International Gas Turbine & Aeroengine Congress & Exhibition
Stockholm, Sweden — June 2–June 5, 1998
This paper has been accepted for publication in the Transactions of the ASME
Discussion of it will be accepted at ASME Headquarters until September 30, 1998

INTRODUCTION

To date, measurement of spectral distributions and length scales in film cooling studies has primarily focused on the freestream. It is common, for instance, to see film cooling studies which document the integral length scales calculated from spectral measurements taken in the freestream. Though the precise influence that freestream scales have on film cooling performance has not been discerned, such documentation has been considered necessary for complete documentation and for proper starting of computational studies. The effect of length scales on cooling performance can only be inferred from data taken in film cooling studies performed at different turbulence levels which were generated by a variety of means.

To complete the documentation and the boundary conditions for computation, details of the scales, energy distribution, and dissipation rates in the coolant flow are needed. Early studies in the literature were primarily with long-hole delivery and, thus, the turbulence was that of fully-developed turbulent pipe flow. As we realize the importance of the hole L/D, and investigate with shorter holes, we raise the need for documenting the influence of the hole and supply plenum geometries on coolant flow velocity distributions, turbulence levels, and scales.

Spectral measurements have been documented in considerable detail over the years for fully-developed turbulent pipe flow, including the studies of Laufer (1953), Lawn (1971), Bremhorst and Walker (1973), and Berman and Dunning (1973). In general, fully-developed pipe flow studies have documented low energy content at low frequencies, a universal -5/3 equilibrium range in the high frequencies, and a majority of the energy containing eddies in a mid-frequency range. Depending upon radial location, integral length scales of 25-75% of the pipe diameter have been determined. The larger scales are measured along the hole centerline while the smaller scales are found nearer the wall. Peak energies were found at $0.3<St_D<1.2$. Spectra in developing pipe flows have been documented by Azad et al. (1978).

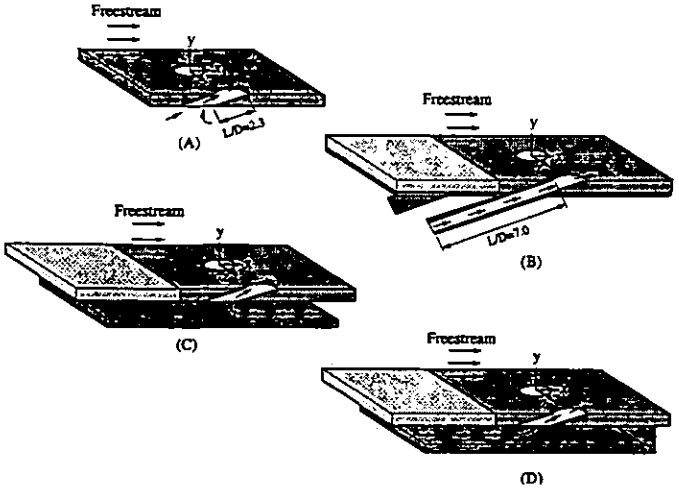

Figure 1: Film Cooling Geometries

Cylinders in cross flows exhibit some similarities to film cooling flows. Like a cylinder in cross flow, the coolant jet is subjected to a freestream cross flow and sheds vortices in its wake. For flow past a solid cylinder, the Strouhal number for $300<Re<100,000$ is nearly constant and equal to 0.21.

Spectral measurements in film cooling flows are few. Coherent frequencies in deflected jets are in the range St_D=0.08-0.085 (McMahon et al., 1971). For an L/D=4.0, Kohli and Bogard (1997) documented spectra of temperature fluctuations along the hole centerline at y/D=0.1 and at different streamwise locations. The characteristic length scale was the hole diameter.

In this paper, spectral energy distributions based on effective velocity are given and corresponding length scales and turbulence parameters are calculated. This is done for film cooling holes of different lengths and coolant supply plenum geometries. The data highlight some fundamental differences from case to case.

EXPERIMENTAL TEST FACILITY

The test facility has two major sections - mainstream and coolant supply systems. The mainstream flow is supplied via a high-turbulence wind tunnel constructed by Wang (1996). The tunnel is a combustor simulator that produces turbulence levels characteristic of those found downstream from the combustor in an actual engine. For reference, the mean velocity and turbulence level in the freestream above the holes are nominally 10.8 m/s and 11.5%, respectively. The boundary layer thicknesses at the film cooling holes are δ_{99}/D=1.13, θ/D=0.082, and δ^*/D=0.105. Some details of the freestream are in Fig. 3 and Table 1. The coolant flow is delivered by a blower to a large plenum (37.5 cm x 66 cm x 17.8 cm) and then to the film cooling test plate. Mass flow to the film cooling holes is monitored with laminar flow meters ($\Delta \dot{m}$=±2.3%). Engine-representative film coolant-to-freestream velocity ratios of 0.5 (Re_D=6,500) and 1.0 (Re_D=13,000) are documented. The nominal density ratio between the two streams is unity. Compressibility effects are not captured in this experiment. Further details of the facility are provided in Burd and Simon (1997) and Burd et al. (1996).

FILM COOLING GEOMETRIES

One row of eleven, streamwise-oriented film cooling holes (Fig. 1(A)) is machined in a 2.54 cm thick phenolic laminate plate to form the film cooling test section. The holes, 19.05 mm diameter and with 35° inclination, have a hole length-to-diameter ratio of 2.3 and a hole pitch-to-diameter ratio of 3.

To investigate the influence of hole length-to-diameter ratio, several sets of tubes of different lengths were connected to the supply plenum-side of the film cooling test plate. The tubes have t/D equal to 0.18. In engines, of course, this ratio would be very large. Entrance loss data of Fried and Idelchik (1989) indicate that the t/D used in this study is large enough that t influences are insignificant. With the tubes, hole length-to-diameter ratios of

4.6, 6.6, and 7.0 are created. The L/D=7.0 tube geometry is machined with its entrance normal to the tube centerline (Fig. 1(B)). The entrance is parallel to the hole exit plane with the L/D=4.6 and 6.6 tubes.

Two additional geometries (Fig. 1(C) and 1(D)), which introduce approach flow momentum, are also investigated. For these geometries, a baffle was placed along the plenum side of the film cooling test plate to restrict the coolant supply flow and force it to enter with a counter-flow (parallel but in the opposite direction, Fig. 1(C)) or co-flow (parallel and in the same direction, Fig. 1(D)) relative to the mainstream. Both have L/D=2.3. Actual engine L/D's range over 1<L/D<10. The total baffle length is 25.3 cm (13.3D) with the entrance to the channel located 10.5 cm (5.5D) upstream from the leading edge of the holes. The delivery channel height is 2D. The film cooling hole-to-channel cross-sectional area ratio is 0.125.

MEASUREMENTS

Single-sensor, hot-wire anemometry (TSI Model 1218-T1.5 connected to a TSI IFA-100 anemometer bridge) is used to measure instantaneous velocity over the exit plane of the film cooling holes. Measurements were with a 3.81 μm diameter hot-wire, with active length-to-diameter ratio of 300, positioned normal to the freestream and parallel to the film-cooled surface (Fig. 2). Thus, the measured velocities are effective cooling velocities to the hot-wire sensor, U_{eff}. Spectral distributions were measured along the streamwise hole centerline at x/D=-0.5, x/D=0.0, and x/D=0.5 of a single hole, of the eleven hole array, as shown in Fig.2. Surveys of velocities over all the holes show hole-to-hole uniformity to within 2%.

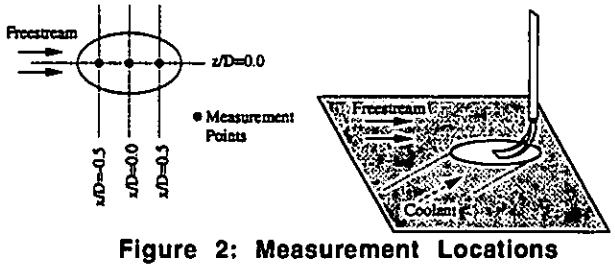

Figure 2: Measurement Locations

For brevity, hole-exit velocity, U_{eff}, and rms turbulence level, u_{eff}, distributions are not presented in this paper. Readers are referred to Burd and Simon (1997,1998) for such measurements. In general, both L/D and flow entry geometry influence hole exit velocity profiles. Short holes exhibit high momentum or "jetting" toward the windward (upstream relative to the freestream) portion of the exit plane whereas longer lengths result in more uniform velocity profiles or slight skewing toward the leeward portion of the exit plane. With short holes, changes in supply plenum geometry influence the location and size of the separation zones that form at the entrance of the film cooling holes. With co-flow, coolant momentum is higher in the leeward portion of the exit plane and with counter-flow, there is substantial "jetting" toward the windward portion of the exit plane.

Film Cooling Spectra

The hot-wire voltage was sampled using a 16-bit analog-to-digital converter (IOTECH Model #ADC 488/8SA) in batch sizes of 262,144. Low-pass filtering was performed using a dual-channel filter (Stanford Research Systems, Inc. Model SR650).

After acquiring data, a fast Fourier transform was performed using Matlab software (The Math Works; Inc.) yielding the power spectral distribution (Hinze,1975).

$$E(f) = \frac{\left[u_{eff}(f, df)\right]^2}{df} \text{ and } E(f) = \frac{2\pi}{U_{eff}} E(\kappa) \qquad (1)$$

Spectral measurements were recorded in four segments then pieced together during post-processing to yield a total of 1.05 million points for each spectral distribution. The sampling frequencies associated with these segments were 20 kHz, 2 kHz, 200 Hz, and 20 Hz. Low-pass filtering for these cases was at 10 kHz, 1 kHz, 100 Hz, and 10 Hz, respectively. This just satisfies the Nyquist sampling criterion. It was not aggressive enough to remove all alias error from the sampled data records. The use of four segments, however, produced large bands of overlap between spectra gathered at different sampling frequencies. Thus, aliases were removed by joining individual segments to produce a single continuous spectrum from the four segments, with only the highest frequency band containing a small amount of alias error. As a check, the sampling frequency was doubled and no appreciable differences were noted. Without smoothing, the spectra distributions would exhibit substantial scatter. Smoothing was employed using Hanning windowing.

The spectral distribution in this paper are presented in two plot formats. The first details P (the product of the power spectral density, E(f), and the local frequency, f, normalized on u_{eff}^2) versus St (e.g. Fig. 3(A)). This type of figure is useful for determining the proportional energy content of the flow at particular frequencies for, in this form, the area under the curve in any frequency band is proportional to the energy in that frequency band. The second type of plot details the power spectral density, E(κ), versus the wave number, κ (e.g. Fig. 3(B)). This plot is useful in determining the dissipation rate and scales within the coolant flow. Examples of the spectra are given in Fig. 3. This figure highlights spectra measured in the freestream. On Fig. 3(B), the various regimes of the spectra can be easily distinguished. At low frequencies, the energy is associated with the largest eddies in the flow and whatever unsteadiness may exist at those frequencies. At high frequencies, the spectra denote the inertial subrange (identified by the $\kappa^{-5/3}$ relationship) and, for higher κ, the dissipation range. At mid frequencies, the spectra distribution is related to the energy-containing eddies in the flow (e.g. peak in Fig. 3(A)). Very low frequency (f<10Hz) spectral data

are not representative of turbulence and merely highlight some low-frequency unsteadiness of the film cooling and mainstream flows.

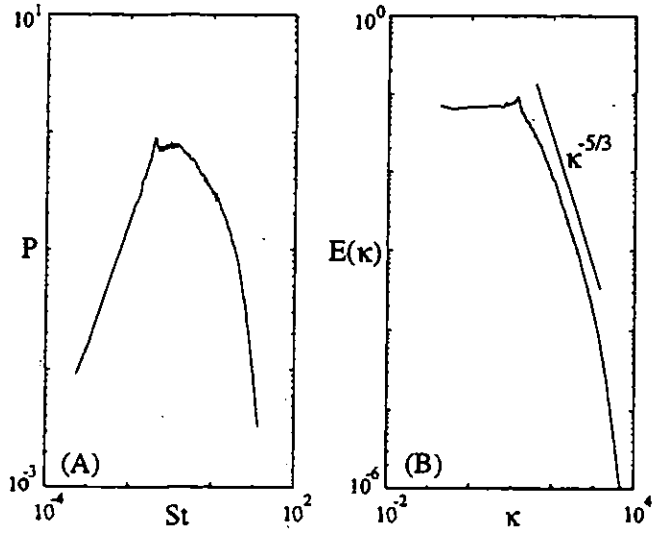

Figure 3: Spectra of Freestream

The single-sample uncertainties involved in single-sensor measurements of velocity are typically larger at smaller velocities. Bias errors result from items such as changes in fluid properties between calibration and measurement, instantaneous flow reversal over the sensor, and sensor drift. A standard propagation, as detailed by Kline and McClintock (1953), of uncertainty contributions which were assigned for these various effects yields a combined uncertainty on time-mean and rms velocity fluctuations of 5-7%. Due to the large sample sizes and long sampling times associated with the hot-wire calibration and measurements, stochastic errors fall well below the deterministic errors and are negligible in comparison. Comparisons of mean velocity and turbulence intensity to data by Laufer (1953), Lawn (1971), Bremhorst and Walker (1973), and Berman and Dunning (1973) in a fully-developed pipe flow are used to corroborate these uncertainty values. Per these data, uncertainty values on the order of 5% of mean values are reasonable under the conditions of the bulk of the present data, so long as velocity fluctuation rms levels remain below 25% of the local measured velocity. Flow reversal over the sensor would be rectified, causing error in both fluctuation magnitude and the indicated frequency. Analyses by Russ and Simon (1990) indicate that such errors become significant for turbulence intensities in excess of 25%. Spectra measurements were taken in flows that did not violate the 25% criterion. The above uncertainties are consistent with previous experience with such measurements and with Yavuzkurt (1984).

Spectra with Varying L/D

Four film cooling hole geometries having L/D=2.3, 4.6, 6.6, and 7.0 with a large, open plenum ("sink" flow delivery, Figs. 1(A) and 1(B)) were investigated to document the effects of hole length.

Figures 4 and 5 show such data (P vs. St) at the hole center (x=y=z=0) with VR=1.0 and 0.5, respectively. It is evident that all the coolant flows exhibit the same dominant frequencies, centered on St=0.8, suggesting turbulent scales on the order of 0.8D. This is similar to the range of scales of temperature fluctuations found by Kohli and Bogard (1997). For the VR=1.0 case, Fig. 4, data from short holes exhibit concentration in a narrower part of that frequency range. Data from long-holes are more typical of fully-developed flows, like those given for the freestream in Fig. 3. Also, peak values are higher with small L/D than with large L/D, suggesting attenuation of some energy with increased hole length. Although not presented, spectral measurements were also taken without the freestream flow. These spectra still exhibit the same range of dominant frequencies, 0.5<St<0.9, for all cases and show the peak to die off as the hole length is increased. It is speculated that this dominant frequency corresponds to the frequency of unsteady separation at the hole entrance and is not associated with any processes in the coolant-mainstream mixing zone.

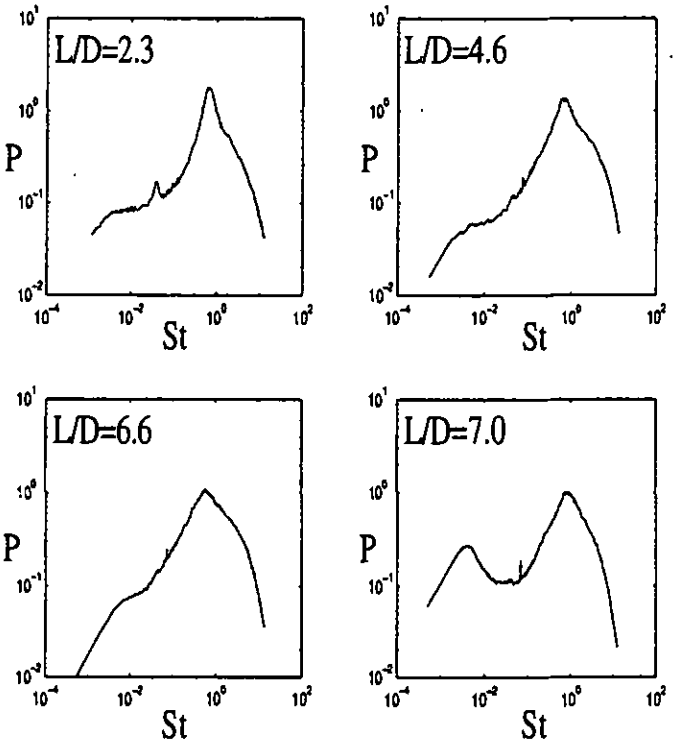

Figure 4: Spectral Distributions at x/D=0 for L/D's at VR=1.0

Recall that the freestream turbulence is centered around St=0.05 (Fig. 3). Noteworthy is that the influence of this low-frequency freestream turbulence (0.02<St<0.07) is small. In the spectra, some low-frequency unsteadiness (St<0.01) is visible. It is most evident for the L/D=7.0 cases, primarily focused at the

windward and center measurement locations, and is measured with and without the external freestream flow. Since this unsteadiness is substantial for L/D=7.0 and minor for L/D=6.6, it is attributed to differences in inlet geometries and the associated separation zones at inlet. Unlike the other cases, L/D=7.0 has no strong preference for the separation location at the inlet. This may make this geometry more susceptible to low-cycle unsteadiness within the coolant supply flow. It is likely that this separation oscillates or precesses.

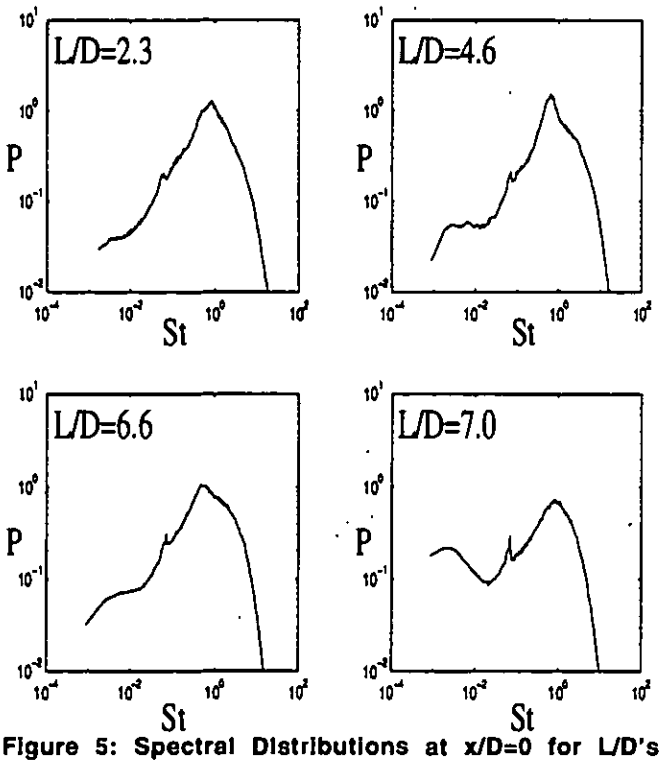

Figure 5: Spectral Distributions at x/D=0 for L/D's at VR=0.5

For VR=0.5 (Fig. 5), trends similar to the VR=1.0 case are observed. With the lower coolant momentum, differences between L/D cases are lessened. The shorter L/D's cases exhibit more peaking of energy, but not to the extent found in Fig. 4. Also, all the peak magnitudes are below those for the VR=1.0 flow. Finally, the VR=0.5 flow cases appear to be more influenced by the freestream, than for VR=1.0 case, since more distinct energy is visible in the $0.02<St<0.08$ range.

Given the distinctly different distributions of exit velocity with different L/D (Burd and Simon,1997 and 1998), it is also likely that spectra may change from one position to another within the emerging jet. To document this, data at y=z=0 were also taken at x/D=-0.5 (upstream of hole center) and x/D=0.5 (downstream of hole center). Figures 6 and 8 highlight these measurements for L/D's of 2.3, 4.6, and 7.0 and VR=1.0.

Upstream, x/D=-0.5, (Fig. 6) there are very distinct differences for different L/D's. Dominant frequencies are visible in each of the coolant flows, but they center about St=0.6 for the short lengths and St=1.0 for L/D=7.0. With such inclined holes, L/D=2.3 and L/D=4.6 cases would be expected to have substantial separation zones and associated shearing at the inlet to the delivery hole whereas the L/D=7.0 case would have a smoother entrance, a smaller vena contracta, and more decay of the effect of this region over the longer delivery length. A sketch of the expected separation zones is shown in Fig. 7. It is apparent from Fig. 6 that the peaks are more defined and larger for L/D=2.3, decreasing as L/D increases. As discussed by Burd and Simon (1997), the shorter L/D cases are more susceptible to "jetting" or having higher velocities in the windward portion of the hole exit plane (See Fig. 7(A)), yielding significantly more coolant mass and turbulence energy in that region. Perhaps the most intriguing aspect of Fig. 6 is found in looking for frequencies that may be associated with the freestream. Both L/D=4.6 and L/D=7.0 cases show very little energy at the freestream frequencies ($0.02<St<0.07$) in their spectral distributions. The L/D=2.3 case has more prominent jetting towards the windward side of the hole (See Fig. 7(B)) and is expected to have more momentum exchange with the freestream in the upstream portion of hole exit plane. Indeed, more influence of the freestream is being "felt" at this upstream location with the short hole, as evidenced by more energy in the $0.02<St<0.07$ range (Fig. 6, L/D=2.3). The interaction is probably not influential, however, for the coolant-energy and freestream-induced-energy peaks remain separated in frequency and the fraction of energy at the freestream-dominant frequency is relatively low.

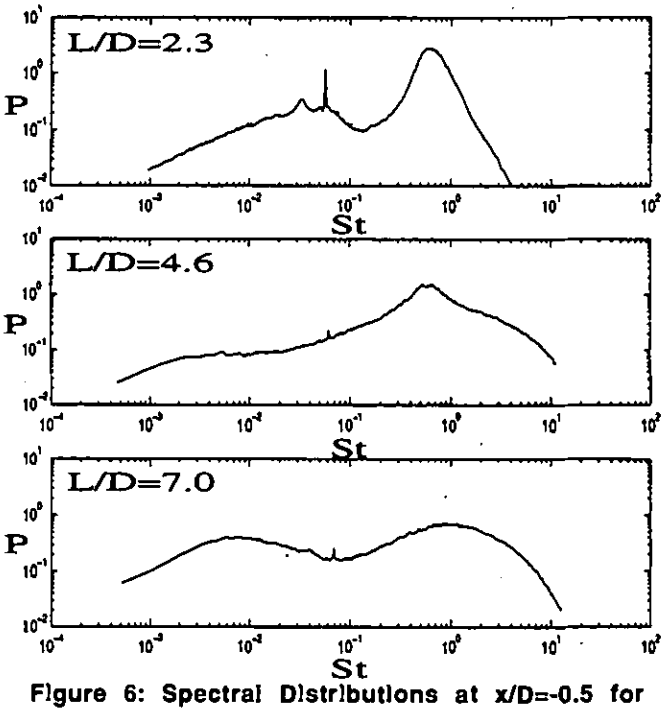

Figure 6: Spectral Distributions at x/D=-0.5 for L/D=2.3, 4.6, and 7.0 and VR=1.0

Measurements leeward of hole center are presented in Fig. 8. Unlike in the upstream measurements, the distributions for all L/D's are similar; all exhibit the majority of their energy content

in the frequency band 0.3<St<3.0 and show little influence of freestream frequencies. Peak energies are centered about St=1.0, suggesting a turbulence scale equal to one hole diameter. As in Figs. 4 and 6, the short L/D cases exhibit more concentrated peak energy. Though a modest contribution, the freestream frequency influence (0.02<St<0.07) appears to increase mildly with L/D.

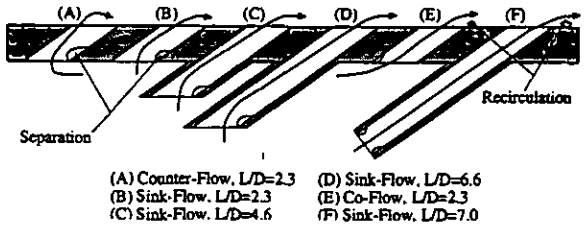

Figure 7: Expected Flow Patterns of Coolant Through Various Hole Geometries

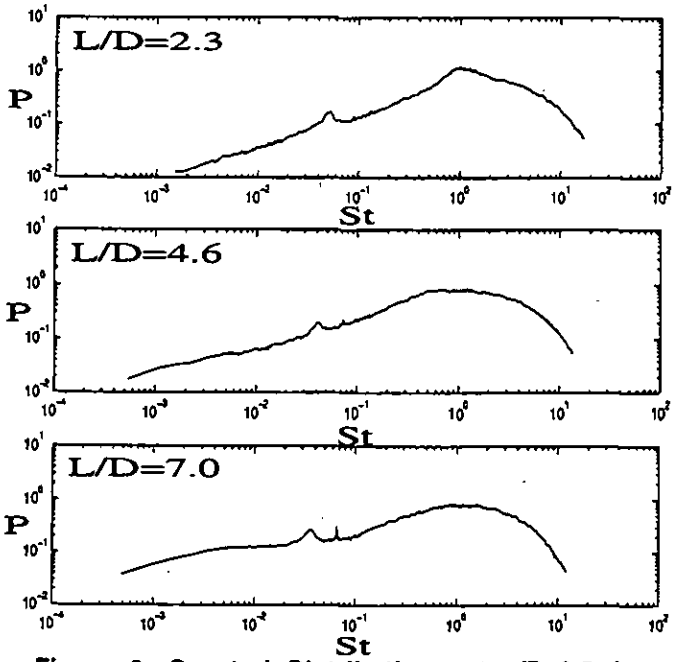

Figure 8: Spectral Distributions at x/D=0.5 for L/D=2.3, 4.6, and 7.0 and VR=1.0

Spectra with Modified Entrance Flow

Spectral distributions (Figs. 9-11) were also taken for film cooling with L/D=2.3 and modified entrance flow (Figs. 1(C) and 1(D)). Corresponding hole-exit velocity distributions for these configurations were presented by Burd and Simon (1997,1998).

In general, the spectra for counter-flow and co-flow are similar to one another at all measurement locations. Contrary to the short-hole, sink-flow configuration, these flows have coolant flow delivered to the holes through a closed channel. As this coolant flow approaches the entrance to the holes, a turbulent boundary layer develops within the channel. This boundary layer is eventually ingested into the hole, contributing mid-frequency energy (St~0.1) to the coolant flow. The net effect is a broader-band spectra for counter- and co-flow, with additional energy in the frequency range 0.005<St<0.4.

Figure 9 highlights the spectral distributions for x/D=-0.5. All cases show a energy peak at St=0.6-0.7. This was previously attributed to unsteady separation at the hole inlet. The peak is less well defined for counter- and co-flow. The counter-flow case has the most prominent "jetting," or skewing of the exit velocity distribution toward the windward portion of the hole, and, thus, is expected to have the highest momentum exchange with the freestream in the upstream portion of hole exit plane (See Fig. 7). Unlike the "sink flow" case, this interaction is strong enough that the freestream (0.02<St<0.07) and coolant peak (St~0.6) energies have merged. With co-flow, the extent of jetting is reduced significantly (Burd and Simon, 1997); thus, coolant-freestream interaction is weaker. As a result, the freestream influence (0.02<St<0.07) is reduced.

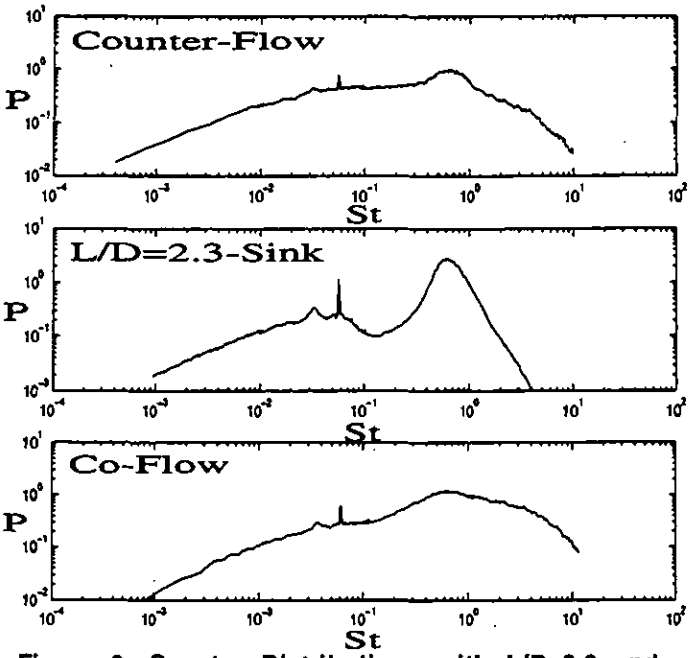

Figure 9: Spectra Distributions with L/D=2.3 and Modified Entrance Flow at x/D=-0.5 and VR=1.0

Distributions at the hole center (x=y=z=0) are in Fig. 10. All configurations still have an energy peak about 0.6<St<0.7, with the "sink flow" configuration being most pronounced. Again, with the channel delivery, counter- and co-flow have more significant energy for St<0.3. Since the coolant jetting and interaction with the freestream is at the windward portion of the hole exit, the energy at the freestream frequencies, 0.02<St<0.07, is reduced at this location.

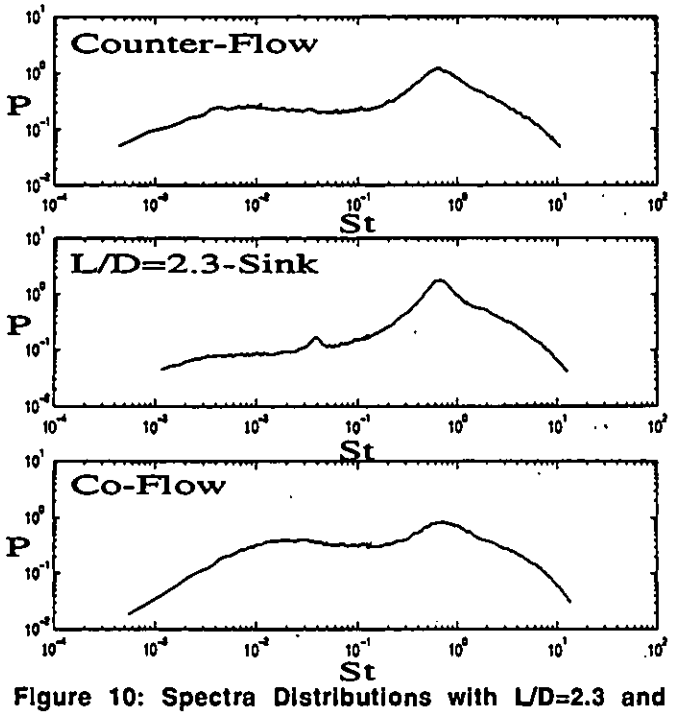

Figure 10: Spectra Distributions with L/D=2.3 and Modified Entrance Flow at x/D=0.0 and VR=1.0

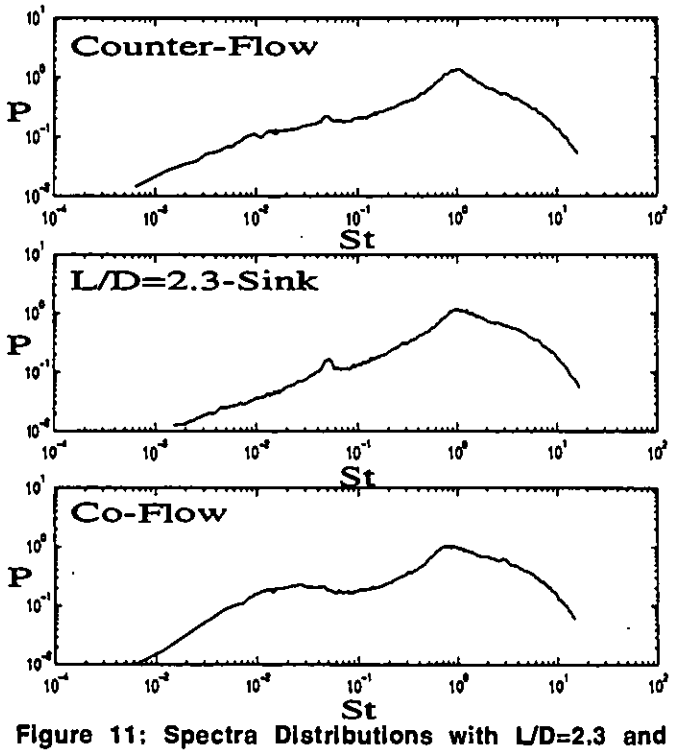

Figure 11: Spectra Distributions with L/D=2.3 and Modified Entrance Flow at x/D=0.5 and VR=1.0

At x/D=-0.5 (Fig. 11), distributions for all the configurations are again similar to one another. Well-defined peak energies are common to all the cases while counter- and co-flow continue to exhibit the broader spectrum. Co-flow exhibits slightly higher energy levels for $0.02<St<0.05$. This suggests that co-flow unsteadiness may be more influenced in the leeward portion of the hole, primarily due to more downstream interaction with the freestream.

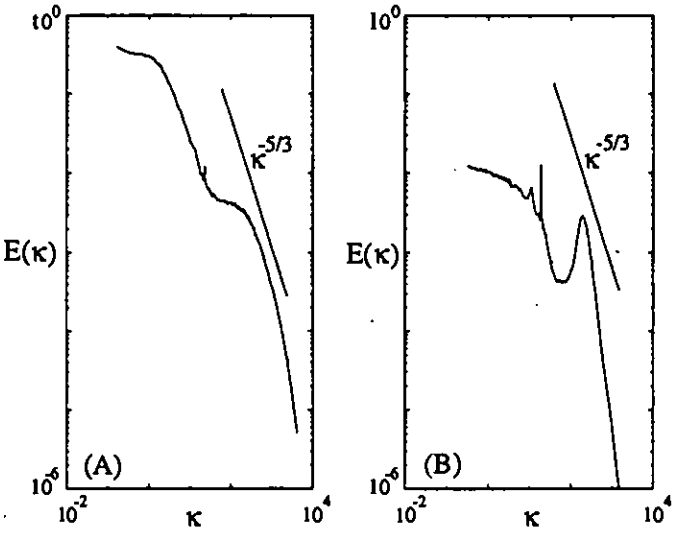

Figure 12: Examples of Spectra for Short and Long-Holes
(A) L/D=7.0, x/D=-0.5, VR=1.0
(B) L/D=2.3, x/D=-0.5, VR=1.0

Turbulence Parameters and Scales

Thus far, normalization has been with the hole diameter. For better understanding and complete documentation, more characterization of the turbulent scales, local turbulent kinetic energy (k), and local dissipation rates (ε) is needed. These quantities are particularly useful in computational modeling using k-ε or large eddy simulation (LES) models.

A common methodology for characterizing length scales in turbulent flows is the integral length scale (Hinze, 1975), a measure of the largest eddies in the flow:

$$\Lambda = \lim_{f\to 0}\left[E(f)\times\frac{U_{eff}}{4\left(u_{eff}\right)^2}\right] = \lim_{\kappa\to 0}\left[E(\kappa)\times\frac{2\pi}{4\left(u_{eff}\right)^2}\right] \quad (2)$$

As $f\to 0$, $E(f)$ typically plateaus.

For long film cooling holes, spectral distributions similar to those shown in Fig. 3(B) are found. Unlike freestream spectra, though, coolant spectra have two regions in which $E(\kappa)$ tend to plateau (Fig. 12). One corresponds to low-frequency unsteadiness ($f\to 0$) and the other is considered to correspond to the larger scales

of turbulence. Length scales computed from Eqn. (2) using $E(\kappa)$ at this second plateau are generally about 0.1-0.5D, characteristic of values found for developing and near-fully-developed pipe flows.

Power spectral density distributions can also be used to determine energy dissipation rates when a -5/3 equilibrium inertial subrange exists (Hinze, 1975). This is done using Eqn. (3) below, in which the dissipation rate is calculated by locating points, $(\kappa,E(\kappa))$, on the spectral distributions that are tangent to a $\kappa^{-5/3}$ line.

$$E(\kappa) = \frac{18}{55} \times 1.62 \times \varepsilon^{2/3} \kappa^{-5/3} \quad (3)$$

The selection of the coefficient 1.62 is consistent with Hinze. Other results may suggest the use of a different empirical value. In using this type of analysis, an assumption of isotropy must be employed. These flows are not expected to be isotropic in the larger scales, but in the inertial subrange, the turbulence is anticipated to be reasonably isotropic. Thus, this model is considered to give a suitable estimate of dissipation when a -5/3 relationship is visible in the power spectra. Dissipation rates are not calculated for several cases with a shorter delivery length, however, as they tended to not follow this relationship. The dissipation rates calculated are listed in Table 1 and are generally observed to be smallest for (1) low VR's and (2) longer film cooling hole lengths. It was previously speculated that these cases have less interaction with the freestream. This speculation is supported by the spectra in Figs. 4, 5, 6, and 8. Also, dissipation values tend to be lowest in the region of highest coolant velocity and lowest turbulence kinetic energy. This generally corresponds to regions in coolant flows where shear is low.

The local turbulence kinetic energy is calculated using the measured rms-velocity fluctuations (Table 1). To determine the local turbulence kinetic energy, k, a formulation which again assumes that the turbulence was isotropic (i.e. that rms-components perpendicular to U_{eff} were also equal to u_{eff}) was used:

$$k = 1.5\left(u_{eff}\right)^2 \quad (4)$$

Observations regarding turbulence kinetic energy are that (1) k magnitudes are largest for short film cooling hole lengths and decrease monotonically as L/D is increased, (2) k scales on VR, and (3) locations of highest coolant momentum tend to have lowest k values.

Knowledge of the turbulence kinetic energy and the dissipation rate provides a means of calculating the energy or dissipation length scale (Hancock and Bradshaw, 1983). Calculated L_u are also provided in Table 1.

$$L_u = \frac{1.5\left(u_{eff}\right)^3}{\varepsilon} = \frac{0.817(k)^{3/2}}{\varepsilon} \quad (5)$$

A final scale that is deduced from the measurements is the Kolmogorov or microscale of turbulence (Table 1):

$$\eta = \left(\frac{\nu^3}{\varepsilon}\right)^{1/4} \quad (6)$$

Several trends are apparent. Energy length scales for all cases tend tn fall into the range $0.1<L_u/D<0.45$. No correlation with parameters emerges. In general, microscales of turbulence are largest for low VR's. No other correlations are clear.

CONCLUSIONS

Spectral distributions have been measured for a variety of film cooling configurations of differing film cooling hole lengths and coolant supply flow orientations. The results highlight some of the fundamental differences. Where possible, physical explanations of the trends were given. The distributions of turbulence energy were dependent on the film cooling design and the measurement location over the exit plane.

In general, coolant flows through long and short holes exhibit nominally the same ranges of peak-energy frequencies. The range of dominant frequencies is $0.5<St<0.9$ for measurements over the upstream portion and center of the bole exit-plane. Slightly larger peak frequencies are evident for flows over the downstream portion of the hole-exit plane ($0.8<St<1.0$). Such dominant frequencies suggest dominant turbulence scales of 0.5-1.0D for coolant flows.

Documentation of additional turbulence parameters, including dissipation rates, and integral, energy, and Kolmogorov length scales, is also presented. In general, these data highlight that short holes have higher dissipation values. Length scales for all geometries tend to be nominally of the same order of magnitude.

Useful for CFD and turbulence modeling is that though energy at the freestream turbulence length scales is visible in the spectra (some spectra show it to be more prominent than others), it never seems to dominate the spectra. This implies that computation of the coolant flow and the freestream-mixing zone could be separated so long as the appropriate velocity distribution of the coolant flow was imposed.

ACKNOWLEDGMENTS

This work is part of a combined study of film cooling with short film cooling holes and lateral injection sponsored by the NASA-Lewis Research Center and Department of Energy, respectively. The NASA project manager is Douglas Thurman. The DOE project is managed by Dr. Daniel Fant of the South Carolina R&D Center.

REFERENCES

Azad, R. S., Arora, S. C., and Reichert, J. K., 1978, "Spectra of Reynolds Stresses in a Developing Pipe Flow," *Proc. of 1978*

Heat Transfer and Fluid Mech. Inst., Pullman, WA, June 26-28, pp. 281-295.

Berman, N. S. and Dunning, J. W., 1973, "Pipe Flow Measurements of Turbulence and Ambiguity Using Laser-Doppler Velocimetry," *J. Fluid Mech.*, Vol. 61, Part 2, pp. 289-99.

Bremhorst, K. and Walker, T. B., 1973, "Spectral Measurements of Turbulent Momentum Transfer in Fully Developed Pipe Flow," *J. Fluid Mech.*, Vol. 61, Part 1, pp. 173-186.

Burd, S. W., Kaszeta, R. W., and Simon, T. W., 1996, "Measurements in Film Cooling Flows: Hole L/D and Turbulence Intensity Effects," ASME Paper 96-WA/HT-7, Accepted for publication in the *ASME Transactions J. Turbomachinery*.

Burd, S. W. and Simon, T. W., 1997, "The Influence on Film Cooling Supply Geometry on Film Coolant Exit and Surface Adiabatic Effectiveness," ASME Paper 97-GT-25.

Burd, S. W. and Simon, T. W., 1998, "Measurements of Discharge Coefficients in Film Cooling," Submitted to 1998 ASME International Gas Turbine Conference, Stockholm, Sweden.

Fried, E. and Idelchik, I. E., 1989, Flow Resistance: A Design Guide for Engineers, Hemisphere Publishing Corp., New York, NY, USA.

Hancock, P. E. and Bradshaw, P., 1983, "The Effect of Free-Stream Turbulence on Turbulent Boundary Layers," *J. Fluids Eng.*, Vol. 105, pp. 284-289.

Hinze, J. O., 1975, Turbulence, McGraw-Hill Book Company, Inc., New York, NY, USA.

Kline, S. J. and McClintock, F. A., 1953, "Describing Uncertainties in Single-Sample Experiments," *Mech. Eng.*, Jan., pp. 3-8.

Kohli, A. and Bogard, D. G., 1997, "Effects of Very High Free-Stream Turbulence on the Jet-Mainstream Interaction in a Film Cooling Flow," ASME Paper 97-GT-121.

Lawn, C. J., 1971, "The Determination of the Rate of Dissipation in Turbulent Pipe Flow," *J. Fluid Mech.*, Vol. 48, Part 3, pp. 477-505.

Laufer, J., 1953, "The Structure of Turbulence in Fully Developed Pipe Flow," NACA Report 1174.

McMahon, H. M., Hester, D. D., and Palfrey, J. G., 1971, "Vortex Shedding from a Turbulent Jet in Crosswind," *J. Fluid Mech.*, Vol. 48, pp. 73-80.

Russ, S. and Simon, T. W., 1990, "Signal Processing using the Orthogonal Triple-Wire Equations," *Flow Lines*, The TSI Quarterly Magazine, Winter.

Walters, D. K. and Leylek, J. H., 1997, "A Detailed Analysis of Film-Cooling Physics, Part 1 - Streamwise Injection with Cylindrical Holes," ASME Paper No. 97-GT-269.

Wang, L., 1996, A Study of Gas Turbine Flows, Turbulence Generation, and Film Cooling Flow Measurement, M.S. Thesis, Department of Mechanical Engineering, University of Minnesota.

Yavuzkurt, S., 1984, "A Guide to Uncertainty Analysis of Hot-Wire Data," *J. Fluids Eng.*, Vol. 106, pp. 181-186.

Table 1: Turbulence Parameters and Scales

Case, Flow	VR	x/D	U_{eff}/U_{bulk}	k (m^2/s^2)	ε (m^2/s^3)	L_t/D	η/D ($x10^3$)
2.3, Sink	0.5	-0.5	1.40	0.186			
		0.0	1.47	1.034	271.8	0.166	3.30
		0.5	1.18	1.788	662.3	0.154	2.64
	1.0	-0.5	1.32	0.306			
		0.0	1.09	8.712	4451	0.248	1.61
		0.5	0.83	5.184	4710	0.107	1.59
4.6, Sink	0.5	0.0	1.24	1.212	295.9	0.193	3.15
	1.0	-0.5	1.20	3.952	1267	0.266	2.18
		0.0	1.00	4.128	1910	0.189	1.97
		0.5	1.01	2.542	1360	0.127	2.14
6.6, Sink	0.5	0.0	1.28	0.724	163.1	0.162	3.74
	1.0	0.0	1.06	2.794	969.6	0.207	2.41
7.0, Sink	0.5	-0.5	1.16	1.108	292.9	0.171	3.18
		0.0	1.33	0.418	25.37	0.456	5.85
		0.5	1.47	0.284	23.63	0.274	5.96
	1.0	-0.5	1.08	1.626	346.0	0.257	3.08
		0.0	1.11	1.402	277.2	0.256	3.25
		0.5	1.32	0.764	225.1	0.127	3.43
2.3, Co-Flow	0.5	0.0	1.30	1.622	401.3	0.220	2.95
	1.0	-0.5	1.21	0.766	211.5	0.136	3.47
		0.0	1.02	10.01	3950	0.344	1.67
		0.5	0.94	5.910	3755	0.164	1.69
2.3, Counter-Flow	0.5	0.0	1.51	0.944	197.1	0.199	3.51
	1.0	-0.5	1.38	1.148			
		0.0	1.27	9.004	3760	0.308	1.68
		0.5	1.16	8.284	8732	0.117	1.36
Freestream	N/A	0.0	N/A	2.124	154.0	0.857	3.77